Arch. Metall. Mater. **69** (2024), 2, 653-660

DOI: https://doi.org/10.24425/amm.2024.149794

A. NAVAKOTI[1], D.S. CHAKRAM[1], M. DASARI[1*]

INFLUENCE OF LITHIUM ON STRUCTURAL PROPERTIES OF LEAD ZIRCONIUM TITANATE (PZT)

Lead Zirconium Titanate (PZT) is a potential piezoelectric material for sensor and transducer applications due to its outstanding piezoelectric coupling near the morphotropic phase boundary (MPB). This is because PZT can switch between tetragonal and rhombohedral phases. PZT is still considered to be one of the piezoelectric materials that has received the greatest amount of attention from researchers and is used the most frequently. Modification with Lithium will improve the piezoelectric properties. In this study, the structural properties and morphological studies of Lead zirconium titanate and Lead zirconium titanate with Lithium modification have been evaluated. Various Scherrer's models and other models, such as the Williamson-Hall model and Size-strain plots model, were used to display the observed fluctuations in crystallite size. Morphological analysis was used to determine the particle size. Graphs showing the distribution of particle sizes were drawn.

Keywords: Ceramics; Monshi Scherrer's model; Crystallite size; Particle size and Optical bandgap

1. Introduction

Lead zirconium titanate (PZT) is regarded as a promising piezoelectric material for sensor and transducer applications due to its remarkable piezoelectric coupling at compositions around the morphotropic phase boundary (MPB) between the tetragonal and rhombohedral phases. PZT is still regarded as one of the most extensively researched and commonly utilized piezoelectric materials. PZT-based materials for a wide range of applications, including transducers, sensors, and dielectric ceramics for capacitors, especially in the area of nonvolatile memory [1-12]. There are numerous energy harvesting devices available today, including conventional solar cells, electromagnetic, electrostatic, triboelectric, and piezoelectric micro-generators [13]. Variable PZT system compositions with various Zr/Ti ratios may be adopted according to the individual requirements for different applications. From an application standpoint, the physical characteristics of PZT have been improved by the addition of different iso-valent, sub-valent (donor type), and super-valent (acceptor type) impurities. PZT is a complex perovskite ABO_3 having various ion replacements at the A and B sites. However, few studies have been undertaken to characterize the effects of doping at the A-site. The primary goal of such compositional changes is to increase its piezoelectric characteristics, mechanical quality factor, and, in certain circumstances, high Curie temperature [14]. Li modification increases piezoelectric properties [15]. The materials were synthesized using the traditional mixed-oxide technique. X-ray diffraction was used to examine the phase purity and crystal structure, and scanning electron microscopy was used to examine the Surface morphology microstructure of the sintered ceramics. In the current study, we reported the structural changes of Lead zirconium titanate with Lithium doping.

2. Experimental

In this work, we have prepared pure $PbZr_{0.6}Ti_{0.4}O_3$ (PZT) and $Pb_{1-x}Li_{2x}Zr_{0.6}Ti_{0.4}O_3$, where X = 0.03 ($Pb_{0.97}Li_{0.06}Zr_{0.6}Ti_{0.4}O_3$) (PLZT) ceramics were prepared by conventional solid-state synthesis. To investigate the influence of Lithium, pure PZT ceramic powders doped with Lithium in A-site. In this case, we have doped Li at x = 0.03 by 2 times, Pb^{+2} ions replaced by 2 times of Li^+ and is associated with charge compensation [16]. The considered precursors PbO (99%), ZrO_2 (99%), TiO_2 (99%) and Li_2CO_3 (99%) in the stoichiometric ratio. And mixed by hand grinding in a mortar and pestle for one hour. Further grinding continued for 7 to 8 hours in the acetone medium. This powder mixture was placed in an alumina crucible and calcined at 900°C for 3 hours. Determined the phase by X-ray diffraction (XRD) analysis. Powder X-ray diffraction performed

[1] GITAM (DEEMED TO BE UNIVERSITY), DEPARTMENT OF PHYSICS, GSS, VISAKHAPATNAM-45, INDIA

* Corresponding author: rajadasari@gmail.com

between 2θ = 10 degrees to 80 degrees. Made 8 mm pellets by applying around 6-7ton pressure to obtain dense ceramics and sintered at 1050°C for 2 hours. UV-Vis-NIR spectra were performed in between the range 200 cm^{-1} to 800 cm^{-1} by using Perkin Elmer, USA. Model: Lamda-950.

3. Results and discussions

The calcined sample is investigated by the BRUKER XRD to verify the phase purity. The X-ray diffraction is performed between 2θ = 10 to 80 degrees. And XRD lines were found to be highly sharp and single, i.e., no splitting of lines was detected, which indicates that the materials maintained greater homogeneity and crystallization. It's been documented in the literature [7,8].

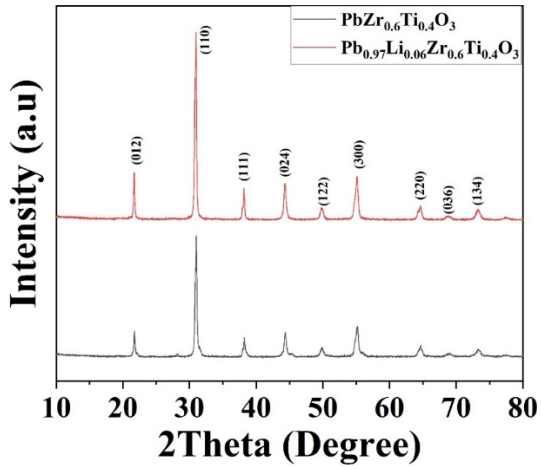

Fig. 1. XRD patterns of PZT and PLZT

The pattern clearly shows the rhombohedral phase. The formation of the phase, either tetragonal or rhombohedral, depends on the sintering temperature [17]. The presence of secondary phases associated with Lithium was not found. Rietveld refinement further confirms the phase and space group by the refinement (Fig. 2).

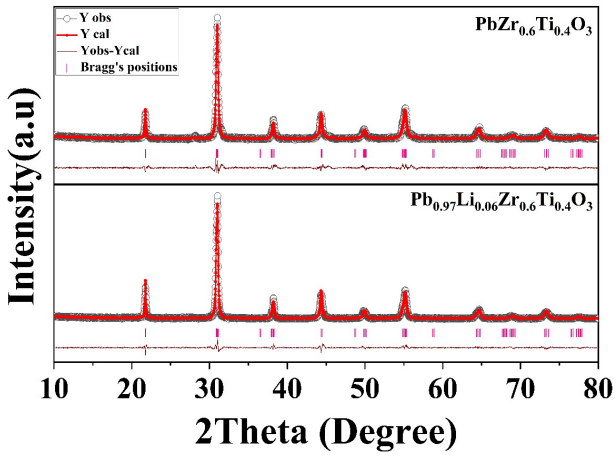

Fig. 2. Rietveld refinement of PZT and PLZT

Lattice parameters and all the obtained output data tabulate from Rietveld refinement. *hkl* values were noted (TABLE 1) and compared to the standard rhombohedral *hkl* values. Obtained chi2 values as 1.8 and 1.6 for PZT and PLZT respectively. Goodness of Fit is 1.3 for both compositions. With Li doping, a decrement in lattice constants was observed. This is because the ionic radius of Lithium 0.76 Å is smaller than that of Lead 1.19 Å. We expected to have higher lattice constants, but we found lower lattice constants in the sample due to lattice shrinkage.

TABLE 1

Different parameters were obtained from Rietveld's refinement of PZT and PLZT

Sample Name	Space group	Lattice parameters	Chi^2	GOF
$PbZr_{0.6}Ti_{0.4}O_3$	R 3 c	a = 5.7615, α = 90° b = 5.7615, β = 90° c = 14.2116, γ = 120°	1.8	1.3
$Pb_{0.97}Li_{0.06}Zr_{0.6}Ti_{0.4}O_3$	R 3 c	a = 5.7591, α = 90° b = 5.7591, β = 90° c = 14.2090, γ = 120°	1.6	1.3

3.1. Determination of crystallite size and strain

3.1.1. Scherrer models

3.1.1.1. Scherrer average model

This approach is named after Swiss scientist Paul Hermann Scherrer. Specifically used to determine the size of crystallites in powder form. In the case of XRD analysis by peak width, which is caused by the instrument's amplification, there will be an increase in crystallite size and micro-strain as well, owing to dislocations [18,19]. The correction of experimental broadening with respect to the corresponding peak will be

$$\beta^2_{corrected} = (\beta^2_{calculated}) - (\beta^2_{experimental}) \quad (1)$$

The crystallite size can be calculated by using Scherrer's Equation. Where D is the crystallite size, K is the shape factor which is 0.89, λ is the wavelength 1.5406Å, θ is the Bragg's diffraction angle, and β is the full width at half maximum (FWHM).

$$D = \frac{K\lambda}{\beta \cos\theta} \quad (2)$$

TABLE 2

Crystallite size PZT and Li-modified PZT

S. No	Sample	Crystallite size D (nm)
1.	$PbZr_{0.6}Ti_{0.4}O_3$	34
2.	$Pb_{0.97}Li_{0.06}Zr_{0.6}Ti_{0.4}O_3$	41

The average crystallite size D is calculated from the Scherrer formula (TABLE 2). The size could be varied with respect to

the method we opted for. Lithium modification resulted in larger crystallites (41 nm vs 34 nm in pure PZT). The further crystallite size was calculated from Sherrer straight line model and another Sherrer model, a straight line passing the origin.

3.1.1.2. Scherrer straight-line model

This is a straight-line model that allows for the simultaneous use of all or selected peaks. In this instance, all peaks were taken into account, and according to the Scherrer equation, plots of $\cos\theta$ against $1/\beta$ (inverse radian unit) for each sample are shown in the Fig., respectively.

$$\cos\theta = \frac{k\lambda}{D}.\frac{1}{\beta} \tag{3}$$

From the Eq. (3), the slope of the plot equals to $\frac{k\lambda}{D}$. The crystallite size values obtained from the slope of the linear fit (Fig. 3) are not valid for naturally occurring nanocrystals since these sizes should all be less than 100 nm. In this instance, this may not apply to bulk samples, but the predicted crystallite sizes of 171 nm and 228 nm for PZT and PLZT, respectively, are bigger than anticipated [20-22].

When the least squares approach is used to fit the data according to the Scherrer equation, it is assumed that the y-intercept has no physical significance. To rectify the application of the Scherrer equation, it is suggested that the linear plot passes through the origin.

3.1.1.3. Straight-line passing the origin in the Scherrer method

In this investigation, a novel model was established. The below Equation was evaluated in order to compel the linear plot to pass through the origin and achieve an acceptable slope for computations. All points from the Fig. 3 were retrieved in this Equation as a plot of y against x points. This is a modification derived from this work for the simultaneous application of the Scherrer equation to all peaks [18].

$$slope = \frac{x_1y_1 + x_2y_2 + \ldots + x_ny_n}{x_1^2 + x_2^2 + \ldots + x_n^2} \tag{4}$$

After calculating slope values as 0.003701, and 0.003043 for PZT and PLZT, the crystallite size is determined as 37 nm and 45 nm, respectively.

TABLE 3

(X, Y) points taken from Fig. 3

$PbZr_{0.6}Ti_{0.4}O_3$		$Pb_{0.97}Li_{0.06}Zr_{0.6}Ti_{0.4}O_3$	
X	Y	X	Y
355.4174	0.98205	450.7043	0.98212
300.0015	0.96361	368.6157	0.9637
264.4941	0.94492	317.7785	0.94505
238.3927	0.92591	281.513	0.92616
217.1199	0.90646	259.108	0.90735
199.7002	0.88629	231.5617	0.88636
171.9794	0.84468	194.1914	0.84509
160.9373	0.82448	180.4461	0.82519
150.2923	0.80205	167.3646	0.80242

3.1.1.4. Modified scherrer method or Monshi-Scherrer method

Monshi et al. [21] presented the following formula after modifying the Scherrer equation.

$$\ln\beta = \ln\left(\frac{k\lambda}{D}\right) + \ln\left(\frac{1}{\cos\theta}\right) \tag{5}$$

By adding least squares to the linear plot, the Monshi-Scherrer approach simplified computation and reduced errors. This route has a condition that the slope must be close to one. The intercept then provides the most precise crystal size. Since ($\beta\cos\theta$) cannot be held constant, the Scherrer equation predicts that nanocrystalline size will rise when *d-hkl* decreases and 2θ increases. Also, the Modified Scherrer equation has the potential benefit of reducing the errors to produce a more precise estimate of crystallite size from all or part of the different peaks [20,21].

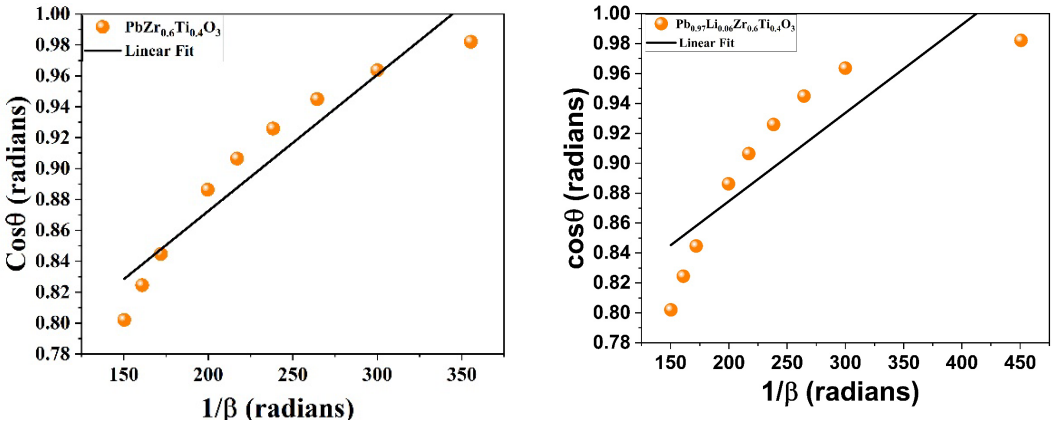

Fig. 3. Scherrer's straight-line model plots for PZT and PLZT

To estimate the crystallite size by the Monshi Scherrer method, the plot of $\ln(1/\cos\theta)$ and $\ln(\beta)$ is plotted on the X and Y axes, respectively. This plot's linear fit can be compared to the straight-line Equation ($y = mx + c$), which resulted in the below equations,

$$\ln\left(\frac{k\lambda}{D}\right) = intercept \tag{6}$$

Considering exponential (e), both sides

$$e^{\ln\left(\frac{k\lambda}{D}\right)} = e^{intercept} \quad \text{then} \quad \frac{k\lambda}{D} = e^{intercept}$$

Crystallite size can be written as $D = \frac{k\lambda}{e^{intercept}}$.

Obtained crystallite size and intercepts indexed in the plots (Fig. 4). This Equation has the benefit of reducing the total absolute error values, $\sum(\pm\Delta \ln\beta)^2$, and providing a single line across the points with a single value of intercept [18-20]. The intercepts of y obtained are –5.83554 and –6.06294 for PZT and PZT modified with Lithium, respectively. Crystallite size calculated is 46 nm and 58 nm for PZT and PZT modified with Lithium, respectively.

3.2. Williamson-hall method

3.2.1. UDM (Uniform Deformation Model)

Crystallite size is the major factor that influences the XRD pattern. On the other hand, two more important parameters that we should consider as influencing factors of the diffraction pattern are lattice strain and lattice defects. In most cases, we can observe this scenario. This method is a simplified integral breath method. The line broadening in this method is isotropic [18-19,23-24]. As a result, it is clear that diffraction domains are also isotropic. Strain-induced can be calculated, and it is

$$\varepsilon = \frac{\beta}{4\tan\theta} \tag{7}$$

Where ε is strain-induced, β is full width at half maximum.

Let us consider that the particle size and strain contribute to line broadening, and they do not depend on each other also, both have a Cauchy-like profile, then we can write line breadth observed is

$$\beta\cos\theta = \frac{K\lambda}{D} + 4\tan\theta \tag{8}$$

From W-H plots, the y-intercept extrapolation gives crystallite size, and the slope provides the strain with induced.

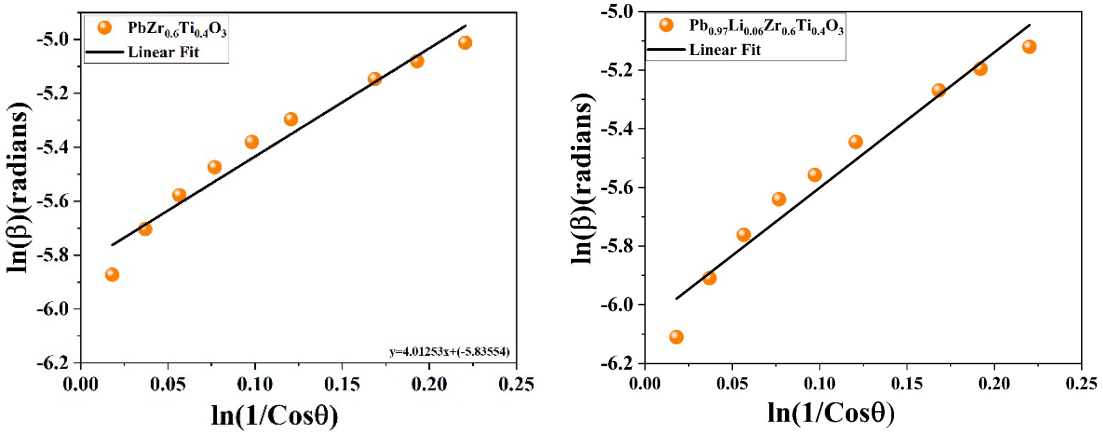

Fig. 4. Modified Scherrer's equation model plots for PZT and PLZT

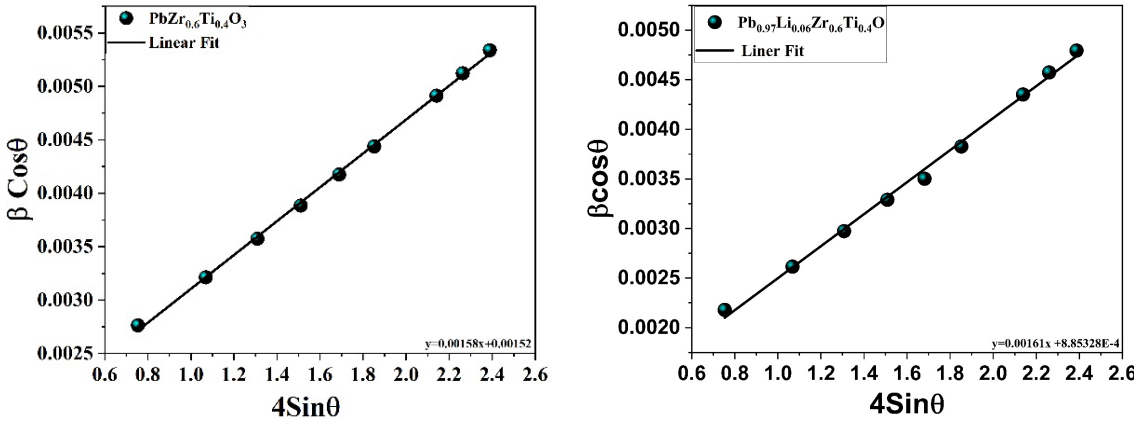

Fig. 5. Williamson-Hall model plots (W-H plots) for PZT and PLZT

Crystallite size from W-H plot (Fig. 5) is 86 nm and 85 nm, which is approximately equal. Strain induced is 0.00152 and 0.00085.

3.3. Size-strain plots

Williamson -Hall method is always contemplating diffraction angle as a function of peak broadening. If we are still looking for more peak profile models of XRD, SSP will be the better one for isotropic functions. As we discussed earlier, there must be a micro-strain contribution as the diffraction domains were isotropic. Size strain plot (SSP) is the method which considers the peak profile as a function of both Lorentz and Gaussian. Size broadening and strain broadening of XRD peak profiles are designated as Lorentz and Gaussian functions, respectively.

$$\beta_{hkl} = \beta_{Lorentz} + \beta_{Gaussian} \tag{9}$$

The above expression represents total peak broadening as a function of both Lorentz and Gaussian.

In general, for the low quality of XRD data, peaks will be overlapped at higher diffracting angles (2θ). As a result, accuracy and precision will be very lower. So, the Size Strain Plot focused on the lower angle reflections, which definitely provides better results for isotropic broadening [21,22].

$$\left(d_{hkl}\beta_{hkl}\cos\theta\right)^2 = k\frac{\lambda}{D}\left(d^2{}_{hkl}\beta_{hkl}\cos\theta\right) + \frac{\varepsilon^2}{4} \tag{10}$$

Where k is the constant, which is dependent on shape.

By the linear fit (Fig. 6) of the graph between $d^2{}_{hkl}\beta_{hkl}\cos\theta$ and $(d_{hkl}\beta_{hkl}\cos\theta)^2$ along the X and Y axis, respectively, we can get a slope which gives average crystallite size and also intrinsic strain from the intercept.

The crystallite size is increased with Lithium modification. The straight-line Equation from the above graph represents the 'm' and y-intercepts. The intercepts obtained are 0.000025, and 0.000021 for PZT and PLZT, respectively indicates intrinsic strain.

TABLE 4

Size and strain from SSP of pure PZT and PLZT

S. No	Sample	Crystallite size *D* (nm)	Intrinsic strain
1.	$PbZr_{0.6}Ti_{0.4}O_3$	54	0.000025
2.	$Pb_{0.97}Li_{0.06}Zr_{0.6}Ti_{0.4}O_3$	72	0.000021

3.4. Scanning electron microscopy

Morphological studies investigated by FESEM and the particle size increased after the lithium modification. In this study, particle size was calculated using Image j software.

It is found that the particle size obtained for PZT is 0.75 µm and for PLZT is 1.13 µm. Due to the excess doping of lithium in place of lead which is associated with charge compensation, could be the reason to obtain increased particle size in doped material than the pure one. The Energy Dispersive Spectrum (EDS) was obtained and shown in Fig. 9. Atomic percentage and weight percentage are presented in the TABLE 5.

TABLE 5

Elemental data of pure PZT and PLZT

Element name	$PbZr_{0.6}Ti_{0.4}O_3$		$Pb_{0.97}Li_{0.06}Zr_{0.6}Ti_{0.4}O_3$	
	Weight %	Atomic %	Weight %	Atomic %
Oxygen (O)	32.97	81.01	25.95	75.08
Titanium (Ti)	4.76	3.90	5.73	5.54
Zirconium (Zr)	13.54	5.83	14.51	7.36
Lead (Pb)	48.74	9.25	53.80	12.02

3.5. Optical bandgap calculation tauc plots

UV-Vis-NIR was performed in between the range of 200 nm to 800 nm to measure the band gap. Fig. 10 shows graph between absorbance and wavenumber. Measured indirect band gap by using the Tauc relation [25].

When a photon of energy, hv, falls on the material, the optical band gap energy of PZT ceramics is computed by consider-

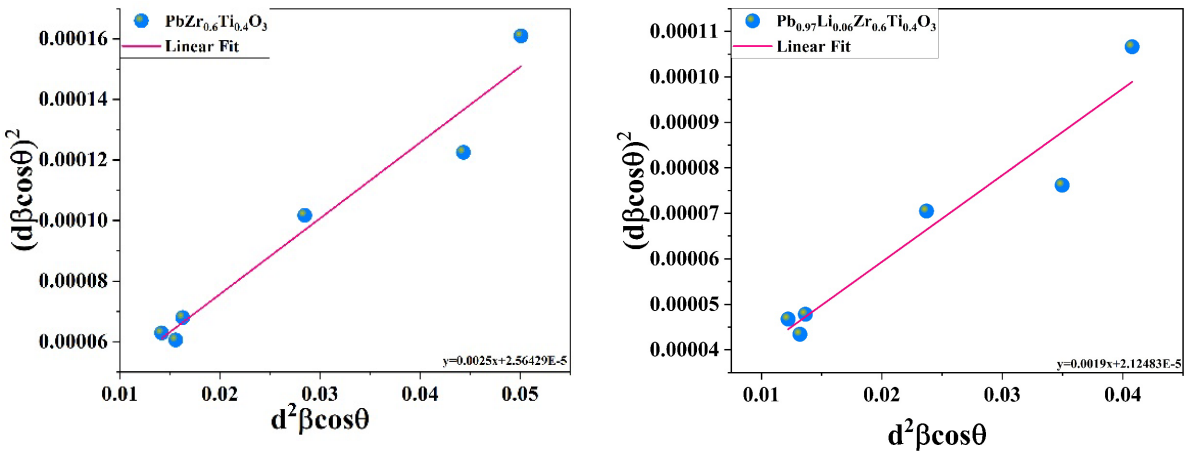

Fig. 6. Linear fit of Size-strain plots of PZT and PLZT

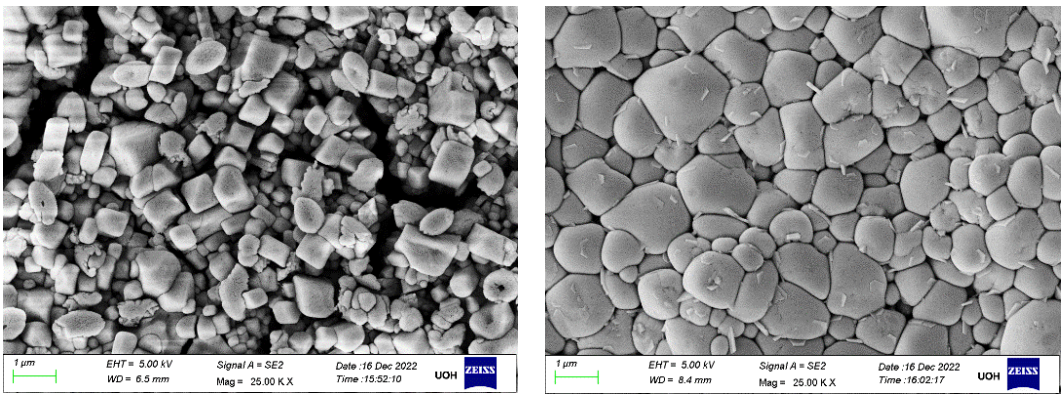

Fig. 7. SEM micrographs of PZT and PLZT

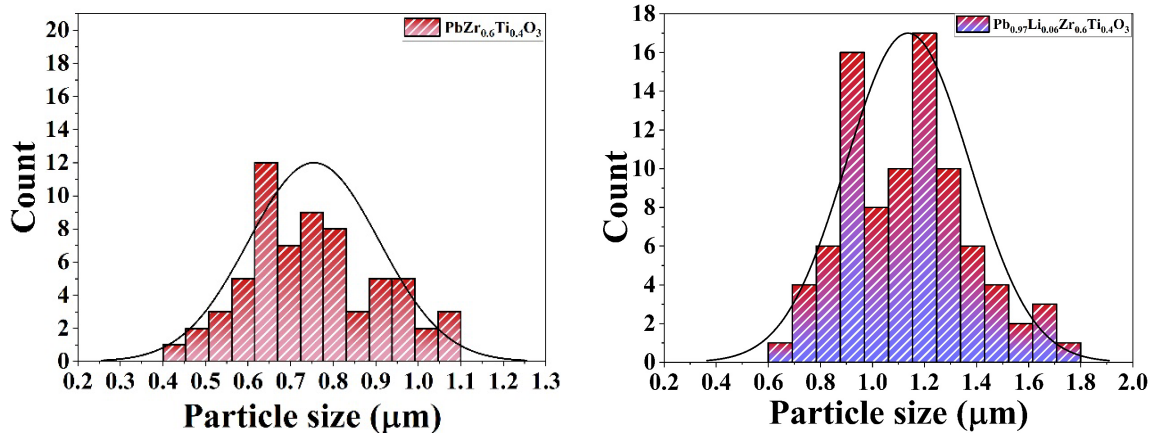

Fig. 8. Particle size distribution plots for PZT and PLZT

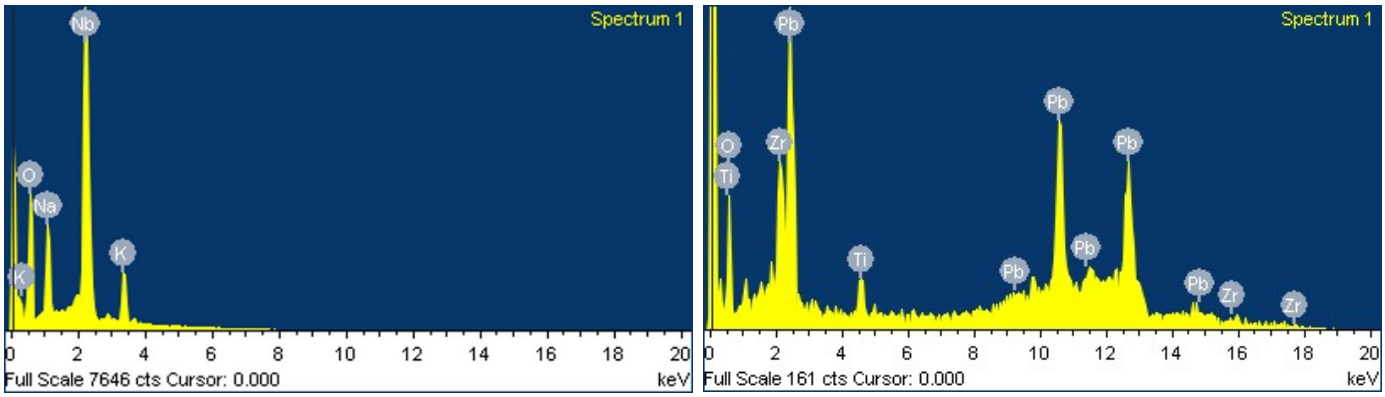

Fig. 9. Energy Dispersive Spectrum (EDS) of PZT and PLZT

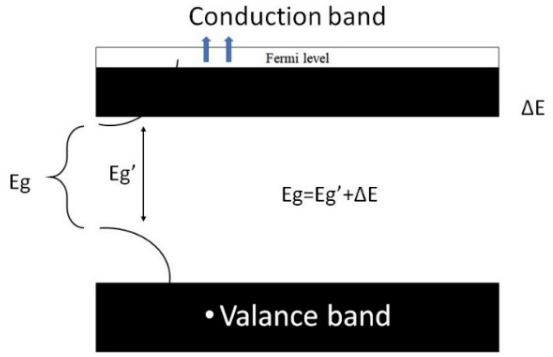

Fig. 10. Band gap and Burstein moss effect

ing a directly allowed electronic transition between the highest occupied state of the valence band and the lowest unoccupied state of the conduction band [26]. Therefore, the absorption coefficient á is related to the optical band gap energy according to the Equation

$$(\alpha h\nu)^2 \propto (h\nu - Eg) \tag{11}$$

Where α is the coefficient of absorption and hν is the energy of the photon. Observed blue shift at 225 nm for Lithium dopant, whereas pure has peak at 227 nm which further leads to Burstein moss shift [27]. There is a blueshift occurred in between 223 nm

to 228 nm mentioned in Fig. 11. This phenomenon occurs as a result of an excess of dopant. When the doping concentration increases, the charge-carriers that occupy the conduction band provide a bandgap *Eg* that is generally smaller than that of the pure material. If the doping concentration increases, the charge-carriers occupy the fermi level, and if the concentration increases further, they begin to move above the fermi level, the band gap is denoted ΔE, and the band gap can be denoted as apparent bandgap $E_{app} = Eg + \Delta E$.

In this particular research article, we did not perform the experiment with low concentrations but directly 2 times of x where x is 0.03, which means $2x = 0.06$. This explanation did not mention in the paper because we did not perform the experiment at low concentration levels. This could be easier if we would have performed experiment at $x = 0.03$.

TABLE 6

Energy band gap comparison

S. No	Sample Name	Band Gap (eV)
1.	$PbZr_{0.6}Ti_{0.4}O_3$	4.6
2.	$Pb_{0.97}Li_{0.06}Zr_{0.6}Ti_{0.4}O_3$	4.7

For PLZT, the optical bandgap calculated is 4.7 eV which is higher than pure PZT, consisting of 4.6 eV.

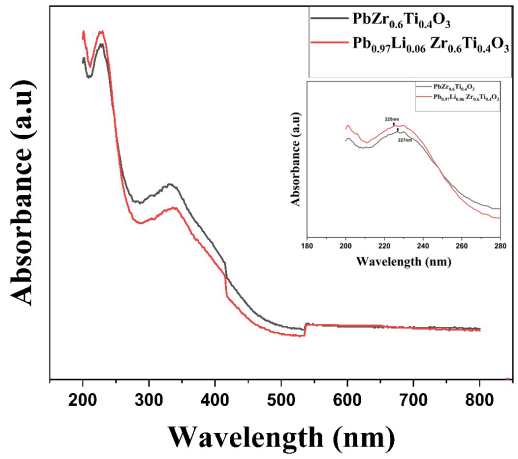

Fig. 11. UV spectrum of PZT and PLZT

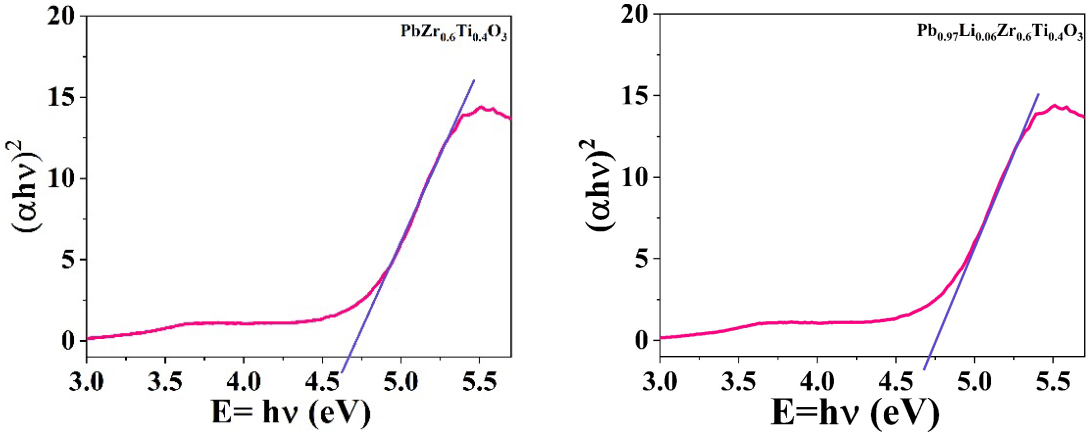

Fig. 12. Tauc plots for PZT and PLZT

4. Conclusion

The structural and morphological properties of lead zirconium titanate and lead zirconium titanate with lithium alteration have been studied. The observed changes in crystallite size were displayed using several Scherrer's models and other models such as the Williamson-Hall model and Size-strain plots model. Modified Scherrer's Equation estimates the precise crystallite size without errors for nano and bulk crystallites. When compared to other models, Williamson-Hall plots provide precise crystallite size in bulk. Morphological studies revealed that the particle size rises as Lithium in lead zirconium titanate is modified. The optical bandgap was investigated, and it was likewise enlarged with Lithium alteration. i.e., from 4.6 eV to 4.7eV. As a result, this Lithium modified PZT may improve both piezoelectric and optical properties.

Acknowledgements

This research work on PZT ceramics was supported by the UGC-DAE Consortium for scientific research, University Campus, Khandwa Road, Indore-452 017. The authors would like to thank UGC-DAE CSR, Indore, for sanctioning the research project and for financial support. We also thank Dr V. Raghavendra Reddy, our mentor and Dr Mukul Gupta of UGC-DAE Consortium for Scientific Research, Indore centre, for extending the measurement facilities XRD. This FESEM with EDAX facility is provided by the School of Physics, University of Hyderabad.

References

[1] H. Jaffe, Piezoelectric ceramics. Journal of the American Ceramic Society **41** (11), 494-498 (1958).

[2] B.V. Hiremath, A.I. Kingon, J.V. Biggers, Reaction Sequence in the Formation of Lead Zirconate-Lead Titanate Solid Solution: Role of Raw Materials. Journal of the American Ceramic Society **66** (11), 790-793 (1983).

[3] S.S. Chandratreya, R.M. Fulrath, J.A. Pask, Reaction Mechanism in the Formation of PZT Solid Solutions. J. Am. Ceram. Soc. **64**, 422-425 (1981).

[4] K.L. Yadav, R.N.P. Choudhary, Piezoelectric properties of modified PZT ceramics. Ferroelectrics **325** (1), 87-94 (2005).

[5] A.J. Bell, On the origin of the large piezoelectric effect in morphotropic phase boundary perovskite single crystals. Applied Physics Letters **76** (1), 109-111(2000).

[6] P. Paruch, T. Tybell, J.M. Triscone, Nanoscale control of ferroelectric polarization and domain size in epitaxial Pb ($Zr_{0.2}Ti_{0.8}$) O_3 thin films. Applied Physics Letters **79** (4), 530-532 (2001).

[7] T.K. Mandal, S. Ram, Synthesis of $PbZr_{0.7}Ti_{0.3}O_3$ nanoparticles in a new tetragonal crystal structure with a polymer precursor. Materials Letters **57** (16-17), 2432-2442 (2003).

[8] R.N.P. Choudhary, J. Mal, Phase transition in Bi-modified PLZT ferroelectrics. Materials Letters **54** (2-3), 175-180 (2002).

[9] H.R. Rukmini, R.N.P. Choudhary, V.V. Rao, Structural and electrical properties of sol–gel prepared (La, Li) modified PZT ceramics. Materials Letters **37** (4-5), 268-275 (1998).

[10] L. Wu, C.C. Wei, T.S. Wu, C.C. Teng, Dielectric properties of modified PZT ceramics. Journal of Physics C: Solid State Physics**16** (14), 2803 (1983).

[11] W. Li, R. Liang, C. Wu, L. Yang, F. Wang, Z. Liu, W. Zhang, Ceramic-Polymer Nanocomposites Design for Energy Storage Capacitor Applications. Advanced Materials Interfaces **9** (32), 2201257 (2022).

[12] V. Raghavendra, P. Viswarupachary, B. Suryanarayana, K.C. Mouli, G.N. V.R. Vikram, N. Murali, Dielectric and piezoelectric properties of Sm3+ doped lead barium niobate (PBN) ceramics. Physica B: Condensed Matter **556**, 75-81, (2019).

[13] J. Le Scornec, R. Seveno, T. Dufay, B. Guiffard, Influence of the intermediate oxidation layer on the characteristics of lead zirconate titanate thin films with aluminium substrate. Thin Solid Films **139761** (2023).

[14] R. Vemuri, B. Suryanarayana, K. Chandra Mouli, P.V. Achary, K.C.V. Rajulu, The effect of Gd3+ doped in lead barium niobate ceramics. In AIP Conference Proceedings (**1992**, 1, 030001). AIP Publishing LLC, (2018, August).

[15] Y. Feng, W.L. Li, D. Xu, W.P. Cao, Y. Yu, W.D. Fei, enhanced piezoelectric properties and constricted hysteresis behaviour in PZT ceramics induced by Li+–Al 3+ ionic pairs. RSC Advances **6** (42), 36118-36124 (2016).

[16] K. Sambasiva Rao, P. Murali Krishna, D. Madhava Prasad, Effect of simultaneous substitution of Li+ and Ti4+ in ceramics of Pb2KNb5O15 on structure, dielectric, modulus, impedance and conductivity properties. Physica Status Solidi (b) **244** (6), 2267-2287 (2007).

[17] P.G. Lucuta, F.L. Constantinescu, D. Barb, Structural dependence on sintering temperature of lead zirconate-titanate solid solutions. Journal of the American Ceramic Society **68** (10), 533-537 (1985).

[18] D. Nath, F. Singh, R. Das, X-ray diffraction analysis by Williamson-Hall, Halder-Wagner and size-strain plot methods of CdSe nanoparticles-a comparative study. Materials Chemistry and Physics **239**, 122021 (2020).

[19] P. Bindu, S. Thomas, Estimation of lattice strain in ZnO nanoparticles: X-ray peak profile analysis. Journal of Theoretical and Applied Physics **8** (4), 123-134 (2014).

[20] M. Rabie, A. Palevicius, A. Monshi, S. Nasiri, A. Vilkauskas, G. Janusas, Comparing methods for calculating nano crystal size of natural hydroxyapatite using X-ray diffraction. Nanomaterials **10** (9), 1627 (2020).

[21] A. Monshi, M.R. Foroughi, M.R. Monshi, Modified Scherrer equation to estimate more accurately nano-crystallite size using XRD. World J Nano Sci Eng **2** (154), 160 (2012).

[22] M.B. Mobarak, M.S. Hossain, F. Chowdhury, S. Ahmed, Synthesis and characterization of CuO nanoparticles utilizing waste fish scale and exploitation of XRD peak profile analysis for approximating the structural parameters. Arabian Journal of Chemistry **15** (10), 104117 (2022).

[23] H. Irfan, K.M Racik, S. Anand, Microstructural evaluation of CoAl2O4 nanoparticles by Williamson-Hall and size-strain plot methods. Journal of Asian Ceramic Societies **6** (1), 54-62 (2018).

[24] A.W. Burton, K. Ong, T. Rea, I.Y. Chan, On the estimation of average crystallite size of zeolites from the Scherrer equation: A critical evaluation of its application to zeolites with one-dimensional pore systems. Microporous and Mesoporous Materials **117** (1-2), 75-90 (2009).

[25] M.C. Rodríguez-Aranda, F. Calderón-Piñar, R. Mayén-Mondragón, J.M. Yáñez-Limón, Synthesis and optical characterization of Pb (Zr0. 53Ti0. 47) O3 thin films on indium tin oxide/quartz substrates by a simplified sol-gel route. Journal of Materials Science: Materials in Electronics **26** (6), 3486-3492 (2015).

[26] S. Yang, D. Mo, X. Tang, Spectroscopic ellipsometry studies of amorphous PZT thin films with various Zr/Ti stoichiometries. Journal of Materials Science **37** (18), 3841-3845 (2002).

[27] P.V. Kamat, N.M. Dimitrijevic, A.J. Nozik, Dynamic Burstein-Moss shift in semiconductor colloids. The Journal of Physical Chemistry **93** (8), 2873-2875 (1989).